Hindawi
Adsorption Science & Technology
Volume 2021, Article ID 5531974, 12 pages
https://doi.org/10.1155/2021/5531974

Research Article

Impact of Na^+ and Ca^{2+} Cations on the Adsorption of H_2S on Binder-Free LTA Zeolites

Annika Starke,[1] **Christoph Pasel**,[1] **Christian Bläker**,[1] **Tobias Eckardt**,[2] **Jens Zimmermann**,[3] **and Dieter Bathen**[1,4]

[1]*University of Duisburg-Essen, Thermal Process Engineering, D-47057 Duisburg, Germany*
[2]*BASF Catalysts Germany GmbH, D-31582 Nienburg, Germany*
[3]*Chemiewerk Bad Köstritz GmbH, D-07586 Bad Köstritz, Germany*
[4]*Institute of Energy and Environmental Technology IUTA e. V., D-47229 Duisburg, Germany*

Correspondence should be addressed to Annika Starke; annika.starke@uni-due.de

Received 28 January 2021; Revised 19 April 2021; Accepted 20 May 2021; Published 30 May 2021

Academic Editor: Diana C. S. Azevedo

Copyright © 2021 Annika Starke et al. This is an open access article distributed under the Creative Commons Attribution License, which permits unrestricted use, distribution, and reproduction in any medium, provided the original work is properly cited.

Hydrogen sulfide is removed from natural gas via adsorption on zeolites. The process operates very effectively, but there is still potential for improvement. Therefore, in this article, the adsorption of hydrogen sulfide was investigated on eight LTA zeolites with different cation compositions. Starting with the zeolite NaA (4 A), which contains only Na^+ cations, the Ca^{2+} cation content was gradually increased by ion exchange. Equilibrium isotherms from cumulative breakthrough curve experiments in a fixed-bed adsorber at 25°C and 85°C at 1.3 bar (abs.) were determined in the trace range up to a concentration of 2000 ppm_{mol}. From a comparison of the isotherms of the different materials, a mechanistic proposal for the adsorption is developed, taking into account the specific positions of the cations in the zeolite lattice when the degree of exchange is increased. The shape of the isotherms indicates two energetically different types of adsorption sites. It is assumed that two mechanisms are superimposed: a chemisorptive mechanism with dissociation of hydrogen sulfide and covalent bonding of the proton and the hydrogen sulfide ion to the zeolite lattice and a physisorptive mechanism by electrostatic interaction with the cations in the lattice. As the degree of exchange increases, the proportion of chemisorption sites seems to decrease. Above an exchange degree of 50%, only evidence of physisorption can be found. It is shown that this finding points to the involvement of weakly bound sodium cations at cation position III in the chemisorption of hydrogen sulfide.

1. Introduction

The amount of natural gas used in 2019 was approx. 24% of the global energy consumption [1]. Forecasts assume an increase in the demand [2]. After production, the gas is transported by pipeline or in cryogenic liquefied form (LNG) [3]. LNG in particular is expected to increase its market share in the coming years [2]. Natural gas consists mainly of methane and other short-chain hydrocarbons. It may also contain higher hydrocarbons, carbon dioxide, and sulfur-containing components. The composition varies depending on the gas exploitation area. When used and transported via pipelines or as LNG, natural gas is subject to strict purity requirements that make it necessary to purify the raw gas. Especially sulfur components such as hydrogen sulfide (H_2S), mercaptans ($C_xH_{x+2}SH$), and carbonyl sulfide (COS) cause problems during transport and use because of their toxic and corrosive properties. This results in an early separation of the sulfur-containing components. Since sulfur components in natural gases are present in trace concentrations, industrial separation takes place by temperature swing adsorption in cyclic fixed-bed processes. Polar adsorbents such as zeolites, silica gels, and silica-alumina gels are often used because they are usually easy to regenerate [4, 5]. Zeolites are preferred for the separation of hydrogen sulfide from natural gas [6]. The adsorption properties of zeolites are strongly dependent on the type and number of cations contained. In addition, zeolites can act as molecular sieves due to their lattice structure, in which cages are connected by window apertures [7, 8]. Today, a large number of zeolite structures are known [9].

In natural gas processing, zeolites with a faujasite structure (FAU) or a Linde-Type-A structure (LTA) are usually used to separate sulfur components. Zeolites have been subject of comprehensive research. For example, adsorption of short-chain hydrocarbons has been considered in many studies. Besides the low capacity, a correlation of carbon chain length and adsorption capacity was found for zeolites of both structures [10–12]. García-Sánchez et al. conducted a simulative study in 2007 to investigate the adsorption of C_1- to C_5-alkanes on LTA zeolites with different sodium/calcium ratios (CaNaA) using Grand Canonical Monte Carlo (GCMC) simulation. An increase in the number of cations in the structure was observed to increase the adsorption of linear alkanes at low and medium pressures. However, a decrease in adsorption was found at the highest pressures. This behavior is explained by different positions of the cations involved in adsorption [13]. The adsorption of H_2S has already been the subject of several research projects. Cruz et al. investigated the adsorption of H_2S on various adsorbents, including FAU zeolites (NaX and NaY) and LTA zeolites (NaA). A higher capacity could be observed on the FAU zeolites. This cannot be correlated with material parameters, and further investigations are necessary to understand the mechanism [14]. In 1996, Yeom et al. determined the crystal structure of a hydrogen sulfide sorption complex on an NaA zeolite using single-crystal X-ray diffraction techniques. At an adsorptive concentration of 93 kPa, 12 H_2S molecules per unit cell could be detected. These molecules arrange themselves at the sodium cations [15]. Karge et al. made a study on the adsorption of H_2S on FAU zeolites (NaX and NaY) using UV/VIS and IR spectroscopy. At low coverings, the results suggest a dissociative adsorption of H_2S on the NaX-zeolite at "strong centers." With increasing coverage, physisorption of undissociated H_2S molecules seems to occur. A much larger adsorption capacity of H_2S can be observed on the NaX zeolite than on the NaY zeolite. As a result, a different adsorption mechanism on the NaY zeolite is suggested [16]. When investigating the adsorption of H_2S on FAU zeolites with systematically varied Si/Al ratios (1.05-3.24) by IR spectroscopy, bands attributable to dissociative adsorption of H_2S could be measured up to a Si/Al ratio of 2.5. Above 2.5, these could no longer be detected. Due to the lower aluminum content, fewer charge-balancing cations are present in the lattice, which results in a different occupation of the cation sites. Thus, dissociative adsorption can be correlated with the number of cations weakly bound to the lattice [17]. Sigot et al. investigated the adsorption of H_2S on NaX zeolites. They observed poor thermal desorption at 350°C. Therefore, a chemisorptive mechanism is proposed, which involves dissolution and dissociation of H_2S in the pore water films of the zeolite with a subsequent oxidation reaction forming elemental sulfur in the pores [18].

For the adsorption of H_2S on LTA zeolites, evidence for dissociative adsorption can also be found. Förster and Schuldt performed an IR spectroscopic study in 1975 to investigate the interactions in the adsorption of H_2S on NaA and $Ca_{4.4}Na_{3.8}A$ zeolites. This revealed a band near 2500 cm^{-1} for both zeolites. For the NaA zeolite, a shift to higher wavenumbers can be observed, and for the $Ca_{4.4}Na_{3.8}A$, the band remains at constant wavenumbers. The authors conclude that during the adsorption of H_2S on the $Ca_{4.4}Na_{3.8}A$ zeolite, other adsorption sites are occupied than for the NaA. Moreover, in the case of NaA, an additional band near 2585 cm^{-1} was found to persist even after 70 h of evacuation at room temperature. Only when the temperature is increased to 475 K does the band disappear, so that it is assigned to a tightly bound SH^- species [19].

During the adsorption of H_2S on cobalt-exchanged LTA zeolites, the distances of the cations to each other were measured by X-ray diffraction techniques and the adsorption sites of the H_2S molecules were determined. The authors argue against dissociative adsorption of H_2S molecules and the occurrence of SH^- ions [20].

Previous studies lack systematic experimental data which are necessary to investigate and describe the assumed adsorption mechanisms more precisely. Especially regarding the influence of the exchangeable cations on the adsorption behavior of sulfur components, only a small data base is available. There are some studies on LTA zeolites that show an increase in adsorption capacity on a calcium-exchanged zeolite CaNaA compared to the zeolite NaA [13, 21–24].

Data on the adsorption of sulfur components on binder-free zeolites are completely missing. Given this fact, the chair of thermal process engineering of the University of Duisburg-Essen investigated the adsorption of H_2S on different adsorbents in cooperation with *BASF Catalysts Germany GmbH* and *Chemiewerk Bad Köstritz GmbH* [25–27]. In this article, we focus on the influence of sodium and calcium ions in LTA zeolites on the adsorption of H_2S. Starting with zeolite NaA, which contains only sodium, the calcium content of the materials was gradually increased. Cumulative breakthrough curves were measured at 25°C and 85°C on a fixed-bed adsorption unit, and adsorption isotherms were determined. From the results, mechanistic suggestions are developed and the influence of different adsorption sites is discussed.

Zeolites consist of SiO_4- and AlO_4-tetrahedra, which are linked together by oxygen atoms. The Si/Al ratio of the LTA zeolites is 1, so that silicon and aluminum atoms are alternately connected via oxygen atoms [28]. The tetrahedra can be combined to secondary building units (SBUs), which form the polyhedral tertiary structure of the zeolites. A typical polyhedron shape is the sodalite cage, consisting of 24 tetrahedra (Figure 1(a)). The crystal lattice of the LTA zeolites consists of sodalite cages connected by two four-membered rings. Eight sodalite cages make up the α-cage with eight-membered rings that form the entrances (Figure 1(b)). There is disagreement in the literature about the symmetry of the crystal lattice [29, 30]. As a consequence, there is an open debate as to whether the Fm3c or Pm3m space group is more appropriate for a description of the crystal lattice. In the fundamental works of Baerlocher et al. [9] and Kulprathipanja [8], both space groups are given for LTA zeolites. So, in this paper, we do not contribute to this discussion but we consider the work of all authors that used one of these two space groups for the evaluation of their XRD data.

Since a negative charge is introduced into the crystal lattice by the aluminum atoms, there are alkali or alkaline earth

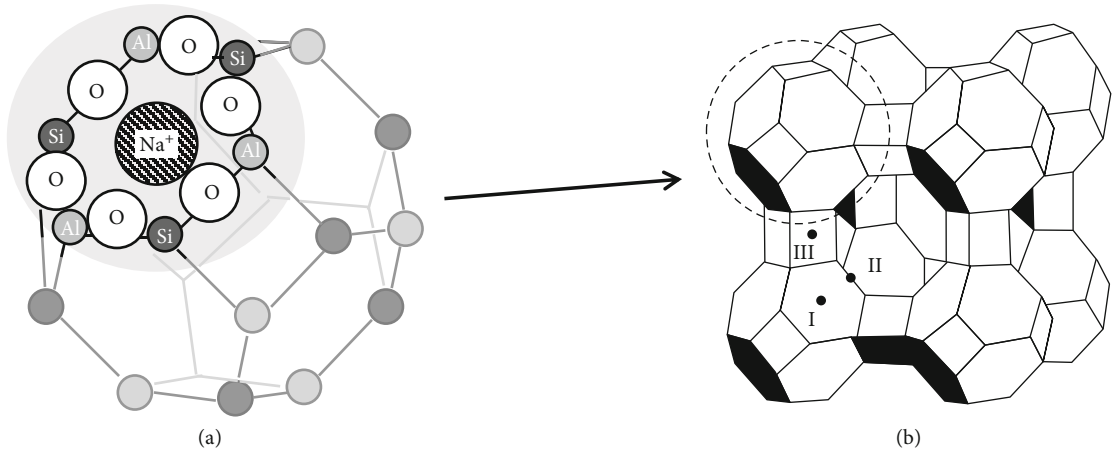

Figure 1: Schematic view of (a) a sodalite cage and (b) an α-cage surrounded by eight sodalite cages.

cations (e.g., Na^+, K^+, Ca^{2+}, and Mg^{2+}) on different cation positions within the α-cage to provide the charge balance. The cations create a polar surface. Three different positions are available to the cations, each resulting in a specific distance to the oxygen atoms. Short distances between the cation and the oxygen atoms lead to a minimization of the free energy. So, the positions with the shortest distance are occupied preferably by the cations. On the other hand, the different distances of the cations to the oxygen atoms allow different spatial arrangements of adsorptive molecules, thus enabling the formation of stronger interactions between the absorbent surface and the adsorptive molecules. Therefore, the individual cation positions provide adsorption sites of different energy values [7, 8, 31, 32].

In Figure 2, the SBUs occurring in the LTA zeolite are shown schematically with the respective cation positions. The oxygen atoms are marked with numbers to distinguish them. Cation position I is within the six-membered ring, eight of them are available per α-cage. In this position, the cations have the smallest distance to the oxygen atoms [20]. Position II is located in the eight-membered ring and thus in the cage entrance. Unlike the cations at position I, the cation at position II is not located in the center of the eight-membered ring, but it is shifted to the edge of the ring (Figure 2). Therefore, cations at this position can have a strong influence on the diffusion of adsorptive molecules [8]. Three type II positions per α-cage can be occupied by cations. Position III is in the four-membered ring. 12 places of position III are available in each α-cage. The positions are occupied by cations in a preferred order, so position I represents the most attractive position for the cations. In the next step, position II and finally position III will be filled [8, 32].

The NaA zeolite has 12 sodium cations in each α-cage. These are distributed among the cation positions. All eight places at position I, all three places at position II, and one place at position III are occupied [34]. During ion exchange with calcium cations, two monovalent sodium cations are exchanged for a divalent calcium cation. This reduces the total number of cations per α-cage [35].

In the following, the materials are distinguished by the "degree of exchange" which describes the percentage of sodium cations removed. Table 1 gives an overview of the materials and their theoretical cation distribution [7, 8, 32]. All materials with calcium cations are labeled with the tag "Ca" in the name.

It is assumed that during ion exchange, the weakest bound cations at position III are first removed from the lattice and the entering divalent cations are deposited at the energetically most favorable position (position I). So, with an increasing degree of exchange, the Na^+ cations are removed according to the sequence III–II–I. At the same time, calcium cations displace still existing sodium cations from the cation position I [36].

2. Materials and Methods

2.1. Apparatus and Procedure. A fixed-bed adsorption unit is used to measure breakthrough curves (Figure 3). Thermal mass flow controllers (MFC) set the concentration of the carrier gas flow and the adsorptive flow. The used flow rate of nitrogen is 10 l min^{-1}, and the flow rate of hydrogen sulfur is between 0.5 ml min^{-1} and 16 ml min^{-1}. The velocity is about 0.15 m s^{-1}. The adsorber column has a diameter of 3.8 cm and a height of 17.5 cm. This corresponds to the general technical design rules with a ratio of 4 : 1 (height to diameter). To reduce wall effects, a value of 19 for the ratio between the adsorber diameter (3.8 cm) and the particle diameter of the adsorbents (2 mm) ensures the recommended ratio of at least >10 [37, 38].

The double-shell design of the adsorber wall allows the temperature control of the adsorber bed using a heated fluid. In addition, the tubes are heated by electrical heating tape. This enables continuous regulation of the process temperature between 25°C and 300°C. Thermal process monitoring is realized with thermocouple type T, which is positioned at regular intervals over the length of the adsorber (five devices). In addition, there is one thermocouple at the outlet and the inlet of the adsorber column. All thermocouples have an accuracy of ±0.5 K. To monitor the pressure in the system, two pressure sensors from *BD Sensors* and an electronic pressure control (EPC) are installed to guarantee an operating pressure of 1.3 bar. The gas mixture is separated by a micro

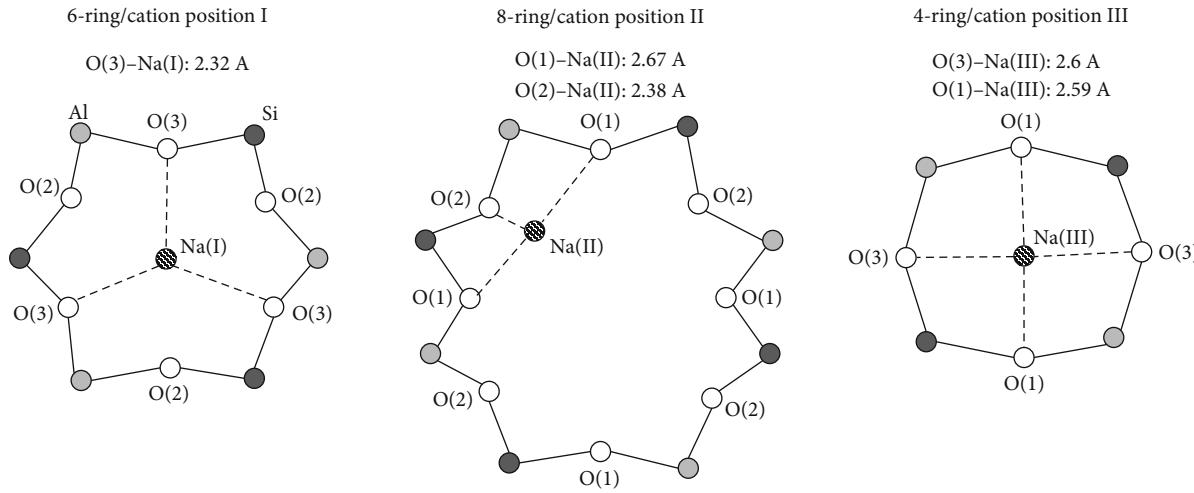

Figure 2: Schematic representation of cation positions I, II, and III according to [33].

Table 1: Theoretical cation distribution in LTA zeolites at different degrees of exchange.

Exchange rate	Number of cations	Position I		Position II		Position III	
0%	12	8		3		1	
		0 Ca^{2+}	8 Na^+	0 Ca^{2+}	3 Na^+	0 Ca^{2+}	1 Na^+
17%	11	8		3			
		1 Ca^{2+}	7 Na^+	0 Ca^{2+}	3 Na^+		
33%	10	8		2			
		2 Ca^{2+}	6 Na^+	0 Ca^{2+}	2 Na^+		
50%	9	8		1			
		3 Ca^{2+}	5 Na^+	0 Ca^{2+}	1 Na^+		
67%	8	8					
		4 Ca^{2+}	4 Na^+				
83%	7	7					
		5 Ca^{2+}	2 Na^+				
100%	6	6					
		6 Ca^{2+}	0 Na^+				

gas chromatograph from *Varian Inc.* (CP-4900) and analyzed by a thermal conductivity detector.

Before each experiment, the adsorbent is conditioned at 300°C for 4 h in an oven under nitrogen atmosphere. 300°C is often used for desorption in the cyclical industrial process of natural gas cleaning. To obtain surface properties similar to those of the industrial process, the desorption temperature of the industrial process is selected as the conditioning temperature for the materials. The residual water content on the zeolite surface after 4 hours is 1.16 wt.% and was determined by Karl-Fischer titration. After the heating, the hot adsorbent is filled into the adsorber and cooled with dry nitrogen until thermal equilibrium reached at the desired temperature. To adjust the concentration, the gas flow is directed via two pneumatically operating valves to the bypass which runs parallel to the adsorber. If constant concentration of the adsorptive can be measured for a period of 30 min, the experiment can be started by redirecting the gas flow to the fixed bed.

As soon as the concentration of the adsorptive at the outlet of the adsorber corresponds to the input concentration and the maximum deviation is within the statistical deviation of the analysis for 45 min, the system has reached the state of equilibrium. Then, the inlet concentration can be raised to measure the next equilibrium point. Using this procedure, cumulative isotherms with 11 equilibrium points were determined.

The equilibrium load X_{eq} can be calculated from the measured breakthrough curves with a mass balance around the adsorber (Eq. (1)). This requires an integration of the area above the breakthrough curves. The mole flow $\dot{n}_{in}$ describes the total material flow which consists of the carrier gas flow and the adsorptive flow. The material flow is related to the mass of the adsorbent m_{ads} to maintain the equilibrium load.

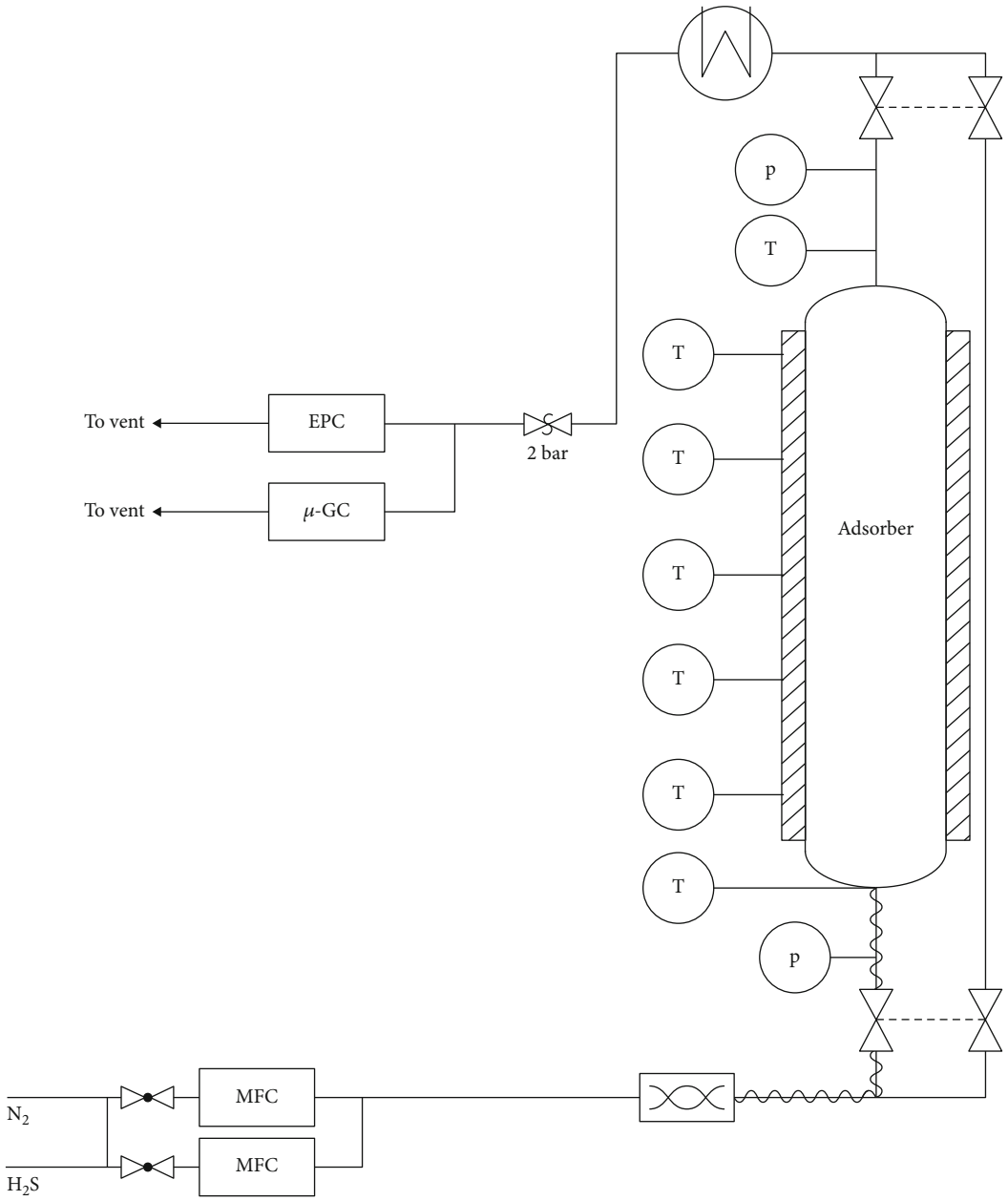

Figure 3: Flow diagram of the experimental adsorber plant ("T" marks the position of the thermocouple type T, and "p" marks the position of the pressure sensors).

The mole fraction y_{in} describes the inlet concentration of the adsorptive, and y_{out} is the measured outlet concentration. The integration requires the sum of the concentration differences over all time intervals Δt_i. Since isothermal measurements use the principle of cumulative measurement, the load of the previous concentration step q_{i-1} must be added for each equilibrium point in the evaluation.

$$X_{\text{eq}} = q_{i-1} + \frac{\dot{n}_{\text{in}}}{m_{\text{ads}}} \sum_{i=1}^{n} \left(\frac{y_{\text{in}} - y_{i,\text{out}}}{1 - y_{i,\text{out}}} \right) \bullet \Delta t_i. \quad (1)$$

Isothermal parameters of the dual-site Langmuir isotherm are fitted to the experimentally determined equilibrium loads (Eq. (2)). The dual-site Langmuir isotherm is an extension of the classic Langmuir isotherm. A second, similar term is added to the first Langmuir term. Thus, it is possible to consider two energetically different adsorption sites. The parameters $X_{\text{mon},1}$ and b_1 represent the monomolecular load and the affinity parameter of the first adsorption site, and $X_{\text{mon},2}$ and $b_2(T)$ represent those of the second adsorption site [39].

$$X_{\text{eq}}(T) = X_{\text{mon},1} \bullet \frac{b_1(T) \bullet y}{1 + b_1(T) \bullet y} + X_{\text{mon},2} \bullet \frac{b_2(T) \bullet y}{1 + b_2(T) \bullet y}. \quad (2)$$

The fitting was performed by nonlinear least-squares

regression analysis using the Levenberg-Marquardt algorithm. The fitted isothermal parameters are given in the supplementary materials.

2.2. Experimental Error. The equilibrium loadings calculated from the experimental data include errors that occur during the experimental procedure due to measurement errors. To calculate the systematic error, the accuracy of the instruments used to determine the mass of the adsorbent (*Acculab 3100.2* balance), the gas concentration (gas chromatograph *Varian Micro GC CP4900*), and the mass flows (mass flow controller *Bronkhorst EL-FLOW*) must be considered. Since the adsorptive volume flows are negligibly small compared to the carrier gas volume flow, only the error of the carrier gas volume flow is relevant. This results in a systematic error of 3.5%. Gaussian error propagation is used to calculate the statistical error. The relevant experimental quantities for the determination of the equilibrium load are the material flow, the adsorbent mass, the time, and the inlet and outlet concentrations of the adsorptive. Due to the precise time recording, the statistical error of time can be neglected. Since the inlet concentration is calculated from the arithmetic mean of the outlet concentration with a large number of measured values, the error on this value is also negligible. This results in a total statistical error of approx. 3.7%. The experimental error was additionally determined by replicate measurements. This resulted in a mean error between 3 and 10%.

3. Materials

The adsorption of H_2S was systematically investigated on eight Linde-Type-A zeolites (LTA zeolites) synthesized by *Chemiewerk Bad Köstritz GmbH*. The zeolites were synthesized from sodium silicate, sodium aluminate, and sodium hydroxide in the liquid phase according to the common synthesis routes [7, 8]. The primary crystals exhibit a size of 2.0 μm–5.0 μm. All investigated zeolites are binder-free (BF) and have a Si/Al ratio of 1. An ion exchange was performed on seven materials, so the zeolites differ in the type and the number of cations they contain. The basic material NaA BF contains only sodium cations for charge balancing. The cation exchange of some sodium cations for calcium cations was done by liquid exchange. In this process, the granulated sodium form of the zeolites was continuously flowed through with the solvent in ion exchange columns. The solvent consisted of water and calcium chloride with a molarity of 0.1-0.5 mol l^{-1} at 298.15 K. The subsequent activation of the zeolites took place at temperatures of approx. 723.15-798.15 K. The degree of exchange indicates the amount of sodium cations removed from NaA BF and exchanged for calcium cations. The examined materials show exchange rates of 19%, 35%, 50%, 70%, 82%, 89%, and 92%. The chemical properties of the zeolites are given in Table S1 in the supplementary materials.

Nitrogen isotherms were recorded volumetrically at 77 K with the measuring device Bel-Sorb Mini from *Bel Japan* for adsorbents with a degree of exchange above 67%. At exchange rates below 67%, cations are still present at cation position II and block the aperture to the α-cage. Therefore, evaluable measurement results can only be obtained at higher exchange rates. For the volumetric measurement, the materials were first conditioned in a vacuum for 6 hours. Table 2 shows the BET specific surface area (DIN ISO 9277) and pore volume according to Gurvich (DIN 66134).

All materials have a similar BET surface (average of 689 m^2 g^{-1}) and pore volume (average of 0.267 cm^3 g^{-1}). Therefore, the BET specific surface area and pore volume for all investigated LTA zeolites are assumed to be independent of the degree of exchange.

Hydrogen sulfide (H_2S > 99.5%, *Air Liquide*) is used as adsorptive. The molar mass of H_2S is 34.08 g mol^{-1}, and the critical molecule diameter is 0.36 nm. H_2S is a polar molecule with a dipole moment of 0.98 D. During adsorption on zeolites, attractive electrostatic cation-dipole interactions between the cations and the hydrogen sulfide molecules and cation-anion interactions between the hydrogen sulfide molecules and the zeolite lattice are expected [40].

The carrier gas is nitrogen and is provided via the university's infrastructure with a purity of 99.999% and a dew point less than -80°C.

4. Results and Discussion

The H_2S isotherms were measured at temperatures of 25°C and 85°C in the concentration range from 50 ppm to 2000 ppm. The loads in (mol kg^{-1}) are plotted versus the gas phase concentration in (ppm_{mol}). The symbols indicate the experimental data, and the lines represent the fitted isotherms. The isothermal parameters are given in Tables S2 and S3, and the measured data points are given in Tables S4 and S5 in the supplementary materials. For reasons of clarity, the error bars are not shown for isotherms at 85°C. All zeolites are binder-free. This is indicated by the abbreviation "BF" in the figures. However, the abbreviation "BF" is omitted in the text for better readability.

4.1. Adsorption of H_2S on LTA Zeolites at 25°C. Figure 4 shows the measured adsorption isotherms of H_2S on the eight investigated LTA zeolites. Based on the shape of the isotherms, the zeolite materials can be divided into two groups. The loads on zeolite NaA and zeolite CaNaA (19%) show a steep increase in capacity in the low concentration range (at approx. 50 ppm). Subsequently, the isotherm flattens out, so that a "kink" is formed and only a small increase in capacity occurs with a further increase in the adsorptive concentration. The materials with this characteristic isotherm form are referred to as "group 1" in the following. The steep isothermal slope at low concentrations points to very strong interactions in adsorption. In the higher concentration range, a flatter increase in capacity is observed, which indicates the formation of weaker interactions. Accordingly, two energetically very different types of adsorption sites can be identified. "Type A" provides a small number of energetically high-quality adsorption sites which are already completely saturated at concentrations of approx. 200 ppm. In contrast, there are many adsorption sites of "type B" that are energetically

Table 2: BET specific surface area and pore volume of the LTA zeolites.

Adsorbent	BET surface ($m^2\ g^{-1}$)	Pore volume ($cm^3\ g^{-1}$)
CaNaA 70% BF	694.1	0.266
CaNaA 82% BF	686.2	0.269
CaNaA 89% BF	695.5	0.269
CaNaA 92% BF	681.1	0.263

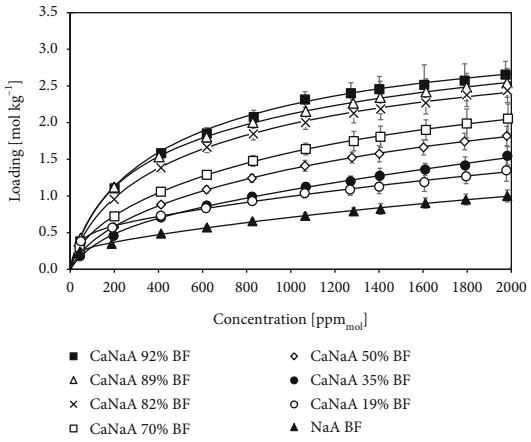

Figure 4: H_2S adsorption isotherms on LTA zeolites of different cation exchange degrees at 25°C.

less valuable. A saturation of these sites cannot be observed in the investigated concentration range.

The adsorption isotherms of H_2S on the materials NaCaA (35%) to NaCaA (92%) have a different isothermal form ("group 2"). Although these isotherms also show a steep increase in capacity with a subsequent flattening of the isotherm at higher concentrations, the decrease of the slope is less pronounced compared to the isotherms of "group 1," so that no kink is visible. The existence of the two energetically very different types of adsorption sites cannot be recognized at exchange rates between 35% and 92%. Therefore, the disappearance of "type A" sites is assumed with an increase of the degree of exchange. Above an exchange degree of 35%, only adsorption sites of "type B" seem to exist. In the high concentration range, an increase in capacity can be observed with an increase in the degree of exchange when the monovalent sodium cations are exchanged for the divalent calcium cations. Due to the higher ionic charge, stronger interactions can be formed between the H_2S molecules and the calcium cations than between the H_2S molecules and the sodium cations. The adsorption sites of "type B" are assigned to physical interactions between the cations in the α-cage and the H_2S molecules.

4.2. Adsorption of H_2S on LTA Zeolites at 85°C. The isothermal field of H_2S at a temperature of 85°C can also be divided into two groups based on the shape of the isotherms (Figures 5 and 6). At 85°C, a similar isothermal form can be found for the materials NaA, CaNaA (19%), and CaNaA (35%) ("group 1," Figure 6(a)). The isotherms exhibit a steep

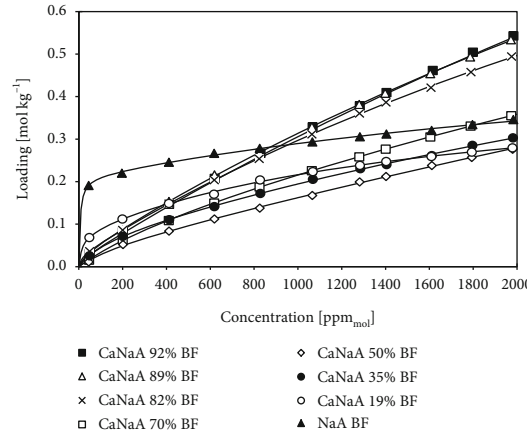

Figure 5: H_2S adsorption isotherm on LTA zeolites of different cation exchange degrees at 85°C.

slope at low adsorptive concentration and then become significantly flatter. This feature is most pronounced for the material NaA and becomes less distinct with increasing degree of exchange. For the zeolites with an exchange degree between 50% and 92%, the isotherms show a uniform slope without characteristic regions ("group 2," Figure 6(b)).

In the low concentration range (up to approx. 600 ppm), a reduction of the capacity can be observed in the order NaA>CaNaA (19%)>CaNaA (35%)>CaNaA (50%). Over the whole concentration range, the material NaCaA (50%) has the lowest capacity for H_2S. In zeolites with an exchange rate above 50%, a strong increase in capacity can be observed when the concentration and exchange rate are increased. The arrangement of the H_2S isotherms is probably due to the superposition of various effects. Figure 7 illustrates the changes that occur in zeolite materials when Na^+ cations are exchanged for Ca^{2+} cations. A degree of exchange of 0% corresponds to the base material NaA, which has only sodium cations. There are 12 sodium cations per α-cage. These are distributed among the cation positions in such a way that all places at positions I (8 cations) and II (3 cations) are completely occupied. One cation per cage occupies one of the 12 available places at position III. The measurement results also indicate 2 different types of adsorption sites: "type A," where strong interactions between the H_2S molecules and the adsorbent can be formed, and "type B," where weaker interactions occur.

Since in the cation exchange process two monovalent sodium cations are exchanged for a divalent calcium cation, the total number of cations per α-cage decreases with increasing degree of exchange. At the same time, the kind of cations changes. If the degree of exchange is below 67%, the sodium cations predominate. At 67%, 4 Na^+ cations and 4 Ca^{2+} cations are present per α-cage, and at exchange levels above 67%, the calcium cations are in the majority. The changes in cation number and species also lead to a change in the occupied places at cation positions I, II, and III. The cations on positions III and II, which are only weakly bound to the lattice, are removed first. A theoretical cation distribution at different degrees of exchange is given in Table 1. According to Eq. (3), the occupation probability of

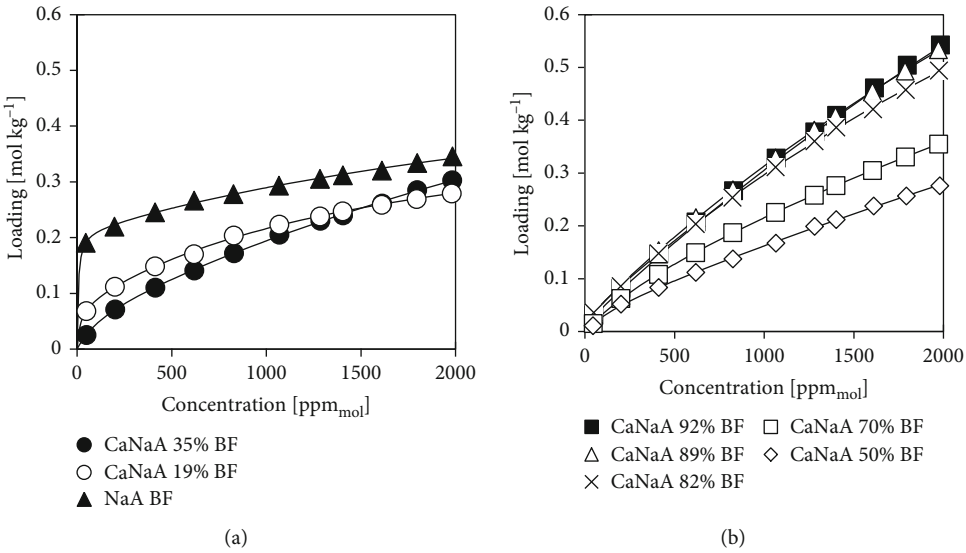

Figure 6: Division of H_2S isotherms at 85°C in (a) group 1 and (b) group 2 based on the shape.

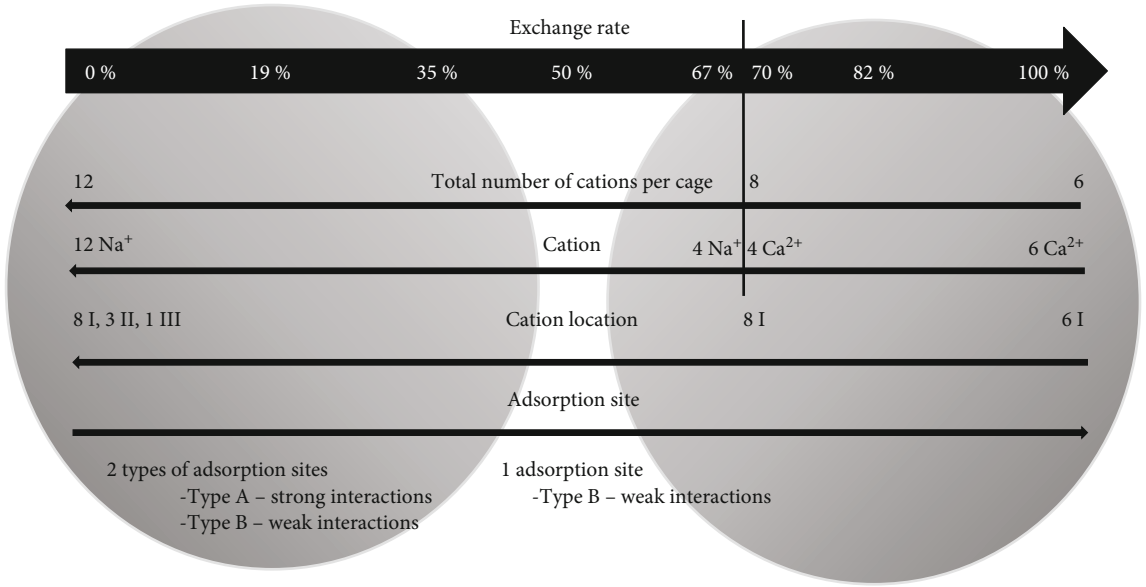

Figure 7: Changes in the α-cage during exchange of Na^+ cations for Ca^{2+} cations.

a site with the energy E, $P(E)$, is proportional to the Boltzmann factor exp $(-E/k\bullet T)$. If two energetically different sites are available, both sites are occupied with different probability. If the energies do not differ very much, as probably in the case of cation positions II and III, no sharp limit can be drawn, from which degree of exchange one place is no longer occupied. Instead, a smooth transition is assumed.

$$P(E) \propto \exp\left(-\frac{E}{k\bullet T}\right). \quad (3)$$

From the changes in the α-cage during cation exchange, it is now possible to discuss the impact of the cations on the adsorption of H_2S.

Also in the adsorption isotherms at 85°C (Figure 5), a capacity-rising effect for zeolites with low exchange rates can be seen in the low concentration range which is again attributed to the presence of "type A" adsorption sites. Since only a small number of these sites are available, there is a saturation at low concentrations. In addition, the number of "type A" adsorption sites seems to become even smaller as the degree of exchange increases, until there is no longer any indication of the presence of type A sites in the CaNaA (50%) material.

For zeolites with high exchange rates, a capacity-increasing effect can be observed in the high concentration range. As with the isothermal field at 25°C, the increase in capacity can also be attributed to the larger number of calcium cations in the α-cage, which leads to strong electrostatic interactions with the H_2S (adsorption sites "type B"). The

material CaNaA (50%) has the lowest capacity over the entire concentration range, since the energetically high-quality adsorption sites of "type A" are no longer available, and at the same time, only a small number of calcium cations are already available. All materials with an exchange degree below 50% benefit from the presence of the adsorption site "type A," while all materials with an exchange degree above 50% benefit from a high calcium content on the adsorption sites of "type B."

4.3. Comparison of H_2S Adsorption on LTA Zeolites at 25°C and 85°C. For a more detailed characterization of the adsorption sites of types A and B, the changes in the adsorption isotherms of the materials NaA and CaNaA (19%) at 25°C and at 85°C are displayed in Figure 8.

For adsorption on zeolite NaA in the low concentration range, a slight reduction of the H_2S capacity by approx. 20% at higher temperatures can be observed. This suggests a low temperature dependence in the low concentration range, where adsorption takes place mainly at the energetically high-quality adsorption sites ("type A"). In the high concentration range, the capacity is reduced by approx. 65% when the temperature is increased from 25°C to 85°C. Since at high concentrations the high-quality adsorption sites are completely saturated, the H_2S molecules at these concentrations adsorb at the energetically less valuable adsorption sites ("type B") provided by the cations in the α-cage. Adsorption at these sites is more dependent on temperature.

With the material CaNaA (19%), on the other hand, a decrease in the capacity for H_2S of 80% can be observed over the entire concentration range when the temperature is increased. From this, it follows that the proportion of nearly temperature-independent adsorption sites ("type A") in CaNaA (19%) zeolite is lower compared to zeolite NaA zeolite. This suggests that the energetically valuable "type A" site is related to the presence of sodium cations at cation position III. These ions are the weakest bound to the zeolite lattice and are the first to be removed from the zeolite during ion exchange. The zeolite NaA has the most cations on position III of all examined zeolites (1 per α-cage). Along with the proceeding cation exchange and the reduction of the total number of cations per α-cage, the cation position III remains increasingly unoccupied.

For all other examined zeolites, a constant reduction in capacity from 25°C to 85°C can also be detected over the entire concentration range.

4.4. Mechanistic Proposal. From the experiments, it is evident that adsorption site "type A" has a high energetic value and is only available in small numbers. The material NaA has the most adsorption sites of "type A." If the degree of exchange is increased, the number of these sites decreases, and above an exchange degree of 50% no more "type A" sites could be detected. Furthermore, the adsorption of H_2S at these adsorption sites is hardly temperature dependent up to a temperature of 85°C. Since with increasing degree of exchange there is less evidence for the energetically high-quality sites, the mechanism for adsorption site "type A" can be correlated with the sodium cations weakly bound to the lattice at position III which are first replaced during ion exchange. Yeom et al. studied a hydrogen sulfide sorption complex on NaA zeolite with XRD techniques and found that the H_2S molecules attach to the cations. The authors propose that one H_2S molecule per α-cage is able to interact with one sodium cation at position III and one sodium cation at position II simultaneously [15]. We do not believe that such a dual interaction is responsible for the adsorption site "type A," as our experimental results argue against it. In particular, we observe a high temperature dependence of the capacity of H_2S on the NaA zeolite in the high concentration range, while in the low concentration range, the temperature dependence is very low. This suggests two clearly different mechanisms. In addition, the NaA zeolite as well as both CaNaA zeolites with exchange efficiencies of 19% and 35% could not be completely desorbed after adsorption of H_2S at 25°C (see Table S6 in the supplementary materials). Therefore, in the low concentration range, we propose a chemisorptive mechanism with a low temperature dependence for adsorption site type A. Figure 9 shows a mechanistic proposal.

First, H_2S physisorbs to the cations in the α-cage. The released adsorption enthalpy supports the dissociation of H_2S molecules into sulfide (SH^-) and a proton (H^+), which are then chemisorptively bound. The sulfide is bound between the sodium cation and an oxygen atom in the zeolite lattice, while the proton interacts with another oxygen atom in the lattice [19, 36, 41]. The same mechanism is considered to cause the catalytic activity in the formation of COS during coadsorption of H_2S and CO_2 on type A zeolites, which is more pronounced at higher sodium contents [41, 42].

Since with increasing degree of exchange there is less evidence for the energetically high-quality sites, the proposed mechanism seems to take place only at the sodium cations weakly bound to the lattice at position III which are first replaced during ion exchange. We assume that the cations located at positions I and II, which may be shielded by the charge of the lattice and are more strongly bound to the lattice, do not take part in the chemisorption [17, 43]. The released adsorption enthalpy is not sufficient to cause the dissociation of the H_2S molecules.

So, with these cations, physisorption occurs. This leads to a superposition of the chemisorptive mechanism on the sodium cations on position III (sites of "type A") and the physisorption on the calcium and sodium cations on positions I and II (sites of "type B").

A high extent of chemisorption takes place in the material NaA, which even dominates when the temperature is increased to 85°C. Physisorption with the material NaA, on the other hand, is only possible on sodium cations and is greatly reduced when the temperature is raised. As soon as calcium cations are introduced into the zeolite, the chemisorption sites disappear and the physisorptive mechanism gets more important. Accordingly, only a small amount of chemisorption can still be detected in the zeolite CaNaA (19%). In addition, this material is subject to physisorption on the calcium cations, so that at 25°C, an increase in capacity can be seen compared to zeolite NaA (Figure 4). For the material CaNaA (35%), a very low chemisorptive effect is

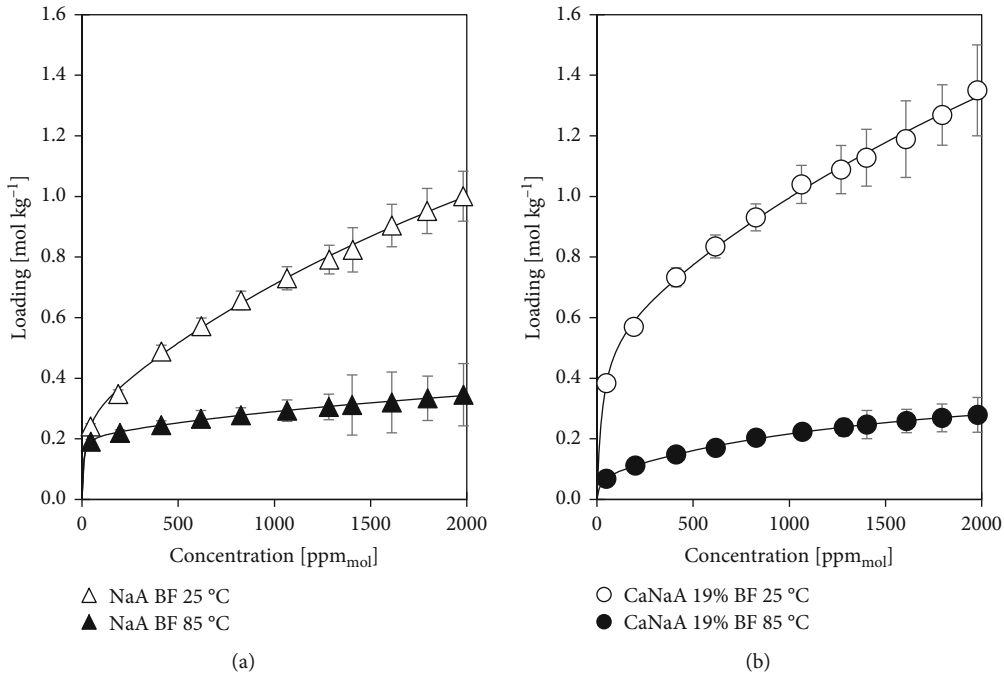

Figure 8: H_2S isotherms at 25°C and 85°C on (a) NaA BF and (b) CaNaA 19% BF.

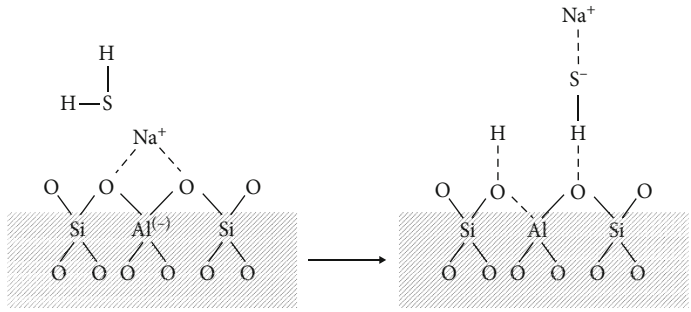

Figure 9: Mechanistic proposal for chemisorptive bonding of H_2S during adsorption on a zeolite surface (adapted from [19]).

only discernible at 85°C, so that a large part of the capacity is provided by physisorptive sites (Figure 5). From a degree of exchange of 50%, there is no more indication of chemisorptive sites and only physisorption takes place at the calcium and sodium cations.

It must be stressed that this mechanistic discussion of H_2S chemisorption is speculative and sketchy, so Figure 9 is merely symbolic.

In the literature, dissociative H_2S adsorption has already been demonstrated by the detection of bound SH^- species on both NaA zeolites and aluminum-rich NaX zeolites [16, 17, 19, 36, 42, 44]. Both zeolite structures have a very similar cation position III (Na^+ cation on the four-ring). In contrast, no chemisorption has yet been detected in the adsorption of H_2S on LTA zeolites exchanged to a high degree with divalent cations [20, 45]. In these materials, cation position III, which is associated with dissociative adsorption of H_2S, is no longer occupied. Thus, no evidence for dissociation of H_2S can be expected. Studies on the dissociative adsorption of H_2S are still lacking for zeolites with low exchange degrees.

In future work, it would be important to support the assumptions found based on the measurement results. By additional X-ray diffraction studies, it would be possible, for example, to detect the cations on their proposed positions. Temperature-programmed desorption experiments could also provide information on the energetic valence of the presumed adsorptive sites. Calorimetric measurements with an instrument suitable for corrosive gases would also be helpful to confirm the chemisorptive mechanism. As a further point of investigation, the influence of residual water on the zeolite surface on the chemisorptive reaction should be considered. The amount of residual water on the surface is so small in our experiments that any influence is neglected. Nevertheless, experiments with systematically varied preloadings of water and H_2S should be carried out.

5. Conclusions

The adsorption of hydrogen sulfide on LTA zeolites with calcium exchange rates of 0%, 19%, 35%, 50%, 70%, 82%, 89%, and 92% was measured at temperatures of 25°C and 85°C.

For this purpose, cumulative breakthrough curves were measured in a fixed-bed adsorption unit and the load was calculated by using a mass balance. Two different isothermal forms were observed at both 25°C and 85°C, indicating two adsorption mechanisms at adsorption sites with significantly different energies.

At low exchange rates (up to approx. 35%), a chemisorptive mechanism is assumed where the hydrogen sulfide is dissociated and the proton and the hydrogen sulfide ion are covalently bound to the zeolite lattice. It is shown that this mechanism involves sodium cations weakly bound to the lattice at cation position III. At higher exchange rates, the sodium cations at this position disappear and a physisorptive mechanism dominates, in which hydrogen sulfide is bound to the cations at different positions in the zeolite lattice via electrostatic interactions.

Data Availability

The underlying data can be found in the Supplementary Material.

Conflicts of Interest

The authors declare that there is no conflict of interest regarding the publication of this paper.

Acknowledgments

The authors wish to express their thanks to BASF Catalysts Germany GmbH for funding and technical support and Chemiewerk Bad Köstritz GmbH for the support with adsorbent materials. We acknowledge support by the Open Access Publication Fund of the University of Duisburg-Essen.

Supplementary Materials

Tables showing chemical properties of zeolite materials (determined by XRF (X-ray fluorescence spectroscopy)), isotherm parameters and regression coefficients, experimental isotherm data, and mass balances for the adsorption and desorption of H_2S at 25°C on NaA, CaNaA (19%), and CaNaA (35%). *(Supplementary Materials)*

References

[1] BP energy economics, "bp Statistical Review of World Energy 2020," 2020, https://www.bp.com/content/dam/bp/business-sites/en/global/corporate/pdfs/energy-economics/statistical-review/bp-stats-review-2020-full-report.pdf.

[2] IEA, *World Energy Outlook 2019*, IEA, Paris, 2019, https://www.iea.org/reports/world-energy-outlook-2019.

[3] F. Berg, C. Pasel, T. Eckardt, and D. Bathen, "Temperature Swing Adsorption in Natural Gas Processing: A Concise Overview," *ChemBioEng Reviews*, vol. 19, no. 4, pp. 59–71, 2019, DOI.

[4] S. Mokhatab and W. A. Poe, *Handbook of Natural Gas Transmission and Processing*, Gulf Professional Pub, Waltham, MA, 2nd edition, 2012.

[5] A. L. Kohl and R. B. Nielsen, *Gas Purification*, Gulf Pub, Houston, TX, 5th edition, 1997.

[6] C. Belviso, *Zeolites-Useful Minerals: Industrial Zeolite Molecular Sieves*, Intech Open, 2016.

[7] R. T. Yang, *Adsorbents: Fundamentals and Applications*, Wiley-Interscience, Hoboken, NJ, 2003.

[8] S. Kulprathipanja, *Zeolites in Industrial Separation and Catalysis*, Weinheim, Wiley-VCH Verlag Gmb H & Co, 2010.

[9] C. Baerlocher, D. Olson, L. B. McCusker, and W. M. Meier, *Atlas of Zeolite Framework Types*, Published on behalf of the Structure Commission of the International Zeolite Association by Elsevier, Amsterdam, Boston, 6th edition, 2007.

[10] R. J. Harper, G. R. Stifel, and R. B. Anderson, "Adsorption of gases on 4A synthetic zeolite," *Canadian Journal of Chemistry*, vol. 47, no. 24, pp. 4661–4670, 1969.

[11] K. F. Loughlin, M. A. Hasanain, and H. B. Abdul-Rehman, "Quaternary, ternary, binary, and pure component sorption on zeolites. 2. Light alkanes on Linde 5A and 13X zeolites at moderate to high pressures," *Industrial and Engineering Chemistry Research*, vol. 29, no. 7, pp. 1535–1546, 1990.

[12] S. Schmittmann, C. Pasel, M. Luckas, and D. Bathen, "Adsorption of light alkanes and alkenes on activated carbon and zeolite 13X at low temperatures," *Journal of Chemical & Engineering Data*, vol. 65, no. 2, pp. 706–716, 2020.

[13] A. García-Sánchez, E. García-Pérez, D. Dubbeldam, R. Krishna, and S. Calero, "A simulation study of alkanes in Linde type A zeolites," *Science and Technology*, vol. 25, no. 6, pp. 417–427, 2007.

[14] A. J. Cruz, J. Pires, A. P. Carvalho, and M. B. de Carvalho, "Physical adsorption of H2S related to the conservation of works of art: the role of the pore structure at low relative pressure," *Adsorption*, vol. 11, no. 5-6, pp. 569–576, 2005.

[15] Y. H. Yeom, Y. Kim, Y. W. Han, and K. Seff, "Crystal structure of a hydrogen sulfide sorption complex of zeolite LTA," *Zeolites*, vol. 17, no. 5-6, pp. 495–500, 1996.

[16] H. G. Karge, M. Ziółek, and M. Łaniecki, "U.v./vis and i.r. spectroscopic study of hydrogen sulphide adsorption on faujasite-type zeolites," *Zeolites*, vol. 7, no. 3, pp. 197–202, 1987.

[17] H. G. Karge and J. Raskó, "Hydrogen sulfide adsorption on faujasite-type zeolites with systematically varied Si-Al ratios," *Journal of Colloid and Interface Science*, vol. 64, no. 3, pp. 522–532, 1978.

[18] L. Sigot, G. Ducom, and P. Germain, "Adsorption of hydrogen sulfide (H2S) on zeolite (Z): Retention mechanism," *Chemical Engineering Journal*, vol. 287, pp. 47–53, 2016.

[19] H. Förster and M. Schuldt, "Infrared spectroscopic study of the adsorption of hydrogen sulfide on zeolites NaA and NaCaA," *Journal of Colloid and Interface Science*, vol. 52, no. 2, pp. 380–385, 1975.

[20] Y. H. Yeom, Y. Kim, and K. Seff, "Crystal structure of a hydrogen sulfide sorption complex of dehydrated partially cobalt(II)-exchanged zeolite A," *The Journal of Physical Chemistry*, vol. 100, no. 20, pp. 8373–8377, 1996.

[21] M. M. Tomadakis, H. H. Heck, M. E. Jubran, and K. Al-Harthi, "Pressure-swing adsorption separation of H_2S from CO_2 with molecular sieves 4A, 5A, and 13X," *Separation Science and Technology*, vol. 46, no. 3, pp. 428–433, 2011.

[22] V. N. Choudary, R. V. Jasra, and T. S. G. Bhat, "Adsorption of nitrogen-oxygen mixture in NaCaA zeolites by elution

chromatography," *Industrial and Engineering Chemistry Research*, vol. 32, no. 3, pp. 548–552, 1993.

[23] D. A. Kennedy, M. Mujcin, E. Trudeau, and F. H. Tezel, "Pure and binary adsorption equilibria of methane and nitrogen on activated carbons, desiccants, and zeolites at different pressures," *Journal of Chemical & Engineering Data*, vol. 61, no. 9, pp. 3163–3176, 2016.

[24] X.-m. Du and E.-d. Wu, "Physisorption of hydrogen in A, X and ZSM-5 types of zeolites at moderately high pressures," *Chinese Journal of Chemical Physics*, vol. 19, no. 5, pp. 457–462, 2006.

[25] B. Steuten, C. Pasel, M. Luckas, and D. Bathen, "Trace level adsorption of toxic sulfur compounds, carbon dioxide, and water from methane," *Journal of Chemical & Engineering Data*, vol. 58, no. 9, pp. 2465–2473, 2013.

[26] V. Chowanietz, C. Pasel, M. Luckas, and D. Bathen, "Temperature dependent adsorption of sulfur components, water, and carbon dioxide on a silica–alumina gel used in natural gas processing," *Journal of Chemical & Engineering Data*, vol. 61, no. 9, pp. 3208–3216, 2016.

[27] V. Chowanietz, C. Pasel, M. Luckas, T. Eckardt, and D. Bathen, "Desorption of mercaptans and water from a silica–alumina gel," *Industrial and Engineering Chemistry Research*, vol. 56, no. 2, pp. 614–621, 2017.

[28] W. Loewenstein, "The distribution of aluminum in the tetrahedra of silicates and aluminates," *American Mineralogist*, vol. 39, pp. 92–96, 1954.

[29] K. Seff and M. D. Mellum, "The silicon/aluminum ratio and ordering in zeolite A," *The Journal of Physical Chemistry*, vol. 88, no. 16, pp. 3560–3563, 1984.

[30] J. M. Adams, D. A. Haselden, and A. W. Hewat, "The structure of dehydrated Na zeolite A (SiAl = 1.09) by neutron profile refinement," *Journal of Solid State Chemistry*, vol. 44, no. 2, pp. 245–253, 1982.

[31] R. Xu, *Chemistry of Zeolites and Related Porous Materials: Synthesis and Structure*, Wiley, Hoboken, NJ, 2010.

[32] K. Seff, "Structural chemistry inside zeolite A," *Accounts of Chemical Research*, vol. 9, no. 4, pp. 121–128, 1976.

[33] J. J. Pluth and J. V. Smith, "Accurate redetermination of crystal structure of dehydrated zeolite A. Absence of near zero coordination of sodium. Refinement of silicon,aluminum-ordered superstructure," *Journal of the American Chemical Society*, vol. 102, no. 14, pp. 4704–4708, 1980.

[34] A. Al Ezzi and H. Ma, "Equilibrium Adsorption Isotherm Mechanism of Water Vapor on Zeolites 3A, 4A, X, and Y," in *Proceedings of the ASME 2017 International Mechanical Engineering Congress and Exposition. Volume 6: Energy*, Tampa, Florida, USA, 2017.

[35] K. Pilchowski, R. Gaedeke, J. Karch, and F. Wolf, "Beitrag zur kationenverteilung und diffusion in 5A-zeolithen," *Kristall und Technik*, vol. 13, no. 1, pp. 47–55, 1978.

[36] M. Bülow, W. Lutz, and M. Suckow, "The mutual transformation of hydrogen sulphide and carbonyl sulphide and its role for gas desulphurization processes with zeolitic molecular sieve sorbents," *Studies in Surface Science and Catalysis*, vol. 120, Part A, pp. 301–345, 1999.

[37] O. Bey and G. Eigenberger, "Fluid flow through catalyst filled tubes," *Chemical Engineering Science*, vol. 52, no. 8, pp. 1365–1376, 1997.

[38] C. N. Satterfield, *Heterogeneous Catalysis in Industrial Practice*, McGraw-Hill chemical engineering books, McGraw-Hill, New York, 2nd edition, 1991.

[39] D. M. Ruthven, *Principles of Adsorption and Adsorption Processes*, Wiley-Interscience Publication, Wiley, New York, 1984.

[40] M. S. Shah, M. Tsapatsis, and J. I. Siepmann, "Hydrogen sulfide capture: from absorption in polar liquids to oxide, zeolite, and metal–organic framework adsorbents and membranes," *Chemical Reviews*, vol. 117, no. 14, pp. 9755–9803, 2017.

[41] V. Chowanietz, C. Pasel, T. Eckardt, A. Siegel, and D. Bathen, "Formation of carbonyl sulfide (COS) on different adsorbents in natural gas treatment plants," *Oil Gas-European Magazine*, vol. 42, no. 2, pp. 82–85, 2016.

[42] P. Fellmuth, W. Lutz, and M. Bülow, "Influence of weakly coordinated cations and basic sites upon the reaction of H2S and CO2 on zeolites," *Zeolites*, vol. 7, no. 4, pp. 367–371, 1987.

[43] K. Möller, *Untersuchung des Adsorptionsverhaltens von Schwefelwasserstoff und einigen Mercaptanen an Zeolithen des Typs X mit Hilfe der Infrarotspektroskopie, [Ph.D. thesis]*, Akademie d. Wiss. d. DDR, 1979.

[44] H. Lechert and H. J. Hennig, "Behavior of proton and na-23 resonance in zeolites of faujasite type in dependence on coating with hydrogen sulfide," *Zeitschrift Fur Physikalische Chemie-Frankfurt*, vol. 76, no. 5-6, pp. 319–327, 1971.

[45] S. B. Jang, M. S. Jeong, Y. Kim, Y. W. Han, and K. Seff, "Crystal structure of a hydrogen sulfide sorption complex of fully Ca^{2+}-exchanged zeolite X," *Microporous and Mesoporous Materials*, vol. 23, no. 1-2, pp. 33–44, 1998.

DuEPublico

Duisburg-Essen Publications online

UNIVERSITÄT DUISBURG ESSEN

Offen im Denken

ub | universitäts bibliothek

This text is made available via DuEPublico, the institutional repository of the University of Duisburg-Essen. This version may eventually differ from another version distributed by a commercial publisher.

DOI: 10.1155/2021/5531974
URN: urn:nbn:de:hbz:464-20210813-113415-9

This work may be used under a Creative Commons Attribution 4.0 License (CC BY 4.0).